

# Robust Space Launcher Control With Time-Varying Objectives

Felix Biertümpfel \*

*Technische Universität, Dresden, Saxony, 01307, Germany*

Julian Theis †

*Airbus Defence and Space, Bremen, Bremen, 28199, Germany*

Harald Pfifer ‡

*Technische Universität, Dresden, Saxony, 01307, Germany*

**This paper presents a novel approach to robust linear time-varying control design for space launchers. It allows the controller to explicitly account for the launcher’s time-varying dynamics and changing control objectives along the ascent trajectory. The latter are readily incorporated via time-varying weighting functions into a mixed sensitivity design. For a traceable and transparent control design, a physically motivated weighting scheme is applied, which requires little tuning effort. The controller is obtained via a novel observer-based finite horizon linear time-varying (LTV) synthesis approach. It provides a transparent structure which is easy to implement. The approach is used to design a pitch controller for a flexible expendable launch vehicle in atmospheric ascent tracking the open-loop guidance reference signal.**

## Nomenclature

$C_A, C_N$	=	aerodynamic force coefficient in axial and normal direction
$d$	=	disturbance vector
$e$	=	error vector
$\mathcal{F}$	=	linear fractional transformation
$F$	=	state feedback gain
$G$	=	generalized plant
$J$	=	moment of inertia, kg m <sup>2</sup>
$K$	=	controller
$L$	=	observer gain

\*Research Associate, Chair of Flight Mechanics and Control, felix.biertuempfel@tu-dresden.de (Corresponding Author). Young Professional Member AIAA

†Guidance, Navigation, and Control Architect, Functional Avionics Engineering & GNC, julian.theis@airbus.com

‡Professor, Chair of Flight Mechanics and Control, harald.pfifer@tu-dresden.de

$Ma$	=	Mach number
$m$	=	mass, kg
$\mathbf{P}$	=	plant model
$\bar{q}$	=	dynamic pressure, Pa
$r$	=	reference signal
$\mathbf{S}$	=	sensitivity function
$T$	=	thrust, N
$t$	=	time, s
$t_f$	=	final time of finite horizon, s
$u, w$	=	input of dynamic system
$\mathbf{W}$	=	dynamic weight
$x$	=	state vector
$y, z$	=	output vector of dynamic system
$\alpha$	=	angle of attack, deg
$\gamma$	=	upper bound on performance metric
$\theta$	=	pitch angle, deg
$\omega$	=	angular frequency, rad/s

## I. Introduction

**T**HE atmospheric ascent of space launchers poses a formidable control problem. It requires the stabilization of an aerodynamically unstable system, the fulfillment of tight tracking constraints, load alleviation to fulfill stringent structural requirements as well as an optimal use of propellant. All these requirements must be fulfilled for constantly changing environmental conditions, rapidly decreasing mass, and thus, varying launcher dynamics. In addition, the launcher is subject to external disturbances, such as wind turbulence.

The state of the art approach to space launcher control is the application of linear time-invariant (LTI) control methods. These methods are applied to design and synthesize single controllers for frozen points in time along the trajectory. The resulting LTI controllers must then be scheduled along the trajectory. Examples for such control designs are gain-scheduled proportional-integral-derivative (PID) controllers [1, 2], linear robust control methods like mixed sensitivity  $H_\infty$  design [3], and nonlinear optimization-based approaches such as structured  $H_\infty$  design [4]. However, these approaches fail to cover the very nature of the ascent problem. The launcher's dynamics are strictly

time-varying over a finite horizon as the vehicle tracks a pre-calculated finite trajectory. LTI methods impose stability and performance metrics on single frozen design points over an infinite time horizon, which contradicts the finite time-varying characteristics of the problem. Most recently, a case was made for linear parameter-varying (LPV) control of space launchers in [5]. Although, LPV control mitigates the ad-hoc scheduling problem, it misses the point that launchers are strictly time-varying and operate on a finite time interval. LPV synthesis considers an infinite horizon with corresponding requirements on stability and performance. It thus suffers from the same disadvantage as its LTI counterpart. Further, an infinite set of possible trajectories is covered, which inevitably introduces conservatism. For verification and validation, finite horizon linear time-varying (LTV) methods have been developed and successfully applied to the launcher ascent problem, see, e.g., [6, 7]. The finite horizon LTV approach actually captures the launcher's behavior. Therefore, finite horizon linear time-varying (LTV) control synthesis presents the logical approach to launcher control. However, no application of robust finite horizon LTV methods for the launcher control problem can be found in literature.

This paper contributes a novel approach to design a structured mixed-sensitivity finite horizon LTV controller for the launcher ascent problem. It explicitly considers the launcher's time-varying dynamics in the controller synthesis over a finite horizon. The synthesis enforces performance only on a specified time horizon rather than over infinite time as LTI and LPV approaches. Hence, classical (infinite time) stability and norm constraints are lifted, which can be taken advantage of for performance gains. The synthesis is conducted using a recently proposed structured mixed sensitivity synthesis for LTV systems [8] presented in Section II. Requiring only the sequential solution of two unidirectionally coupled Riccati differential equations (RDEs), it is computationally more efficient than state-of-the-art approaches, see, e.g., [9]. Moreover, it provides a controller with a transparent pre-defined structure making it particularly easy to implement. The control design is performed for a representative launcher model including flexible modes, which is introduced in Section III. A highly traceable weighting scheme is applied, which is presented in Section III and was first introduced in [10]. Time-varying weights represent changing control objectives along the ascent trajectory, which are mainly imposed by the rapidly changing dynamic pressure. Similar ideas were used in, e.g., [11] and [12], where varying weights represent uncertainties. The controller is validated via simulation using a high fidelity nonlinear simulator in Section V. The simulations are conducted over a large set of perturbed launcher dynamics and realistic wind turbulence as encountered by the launcher during ascent.

## **II. Background on Linear Time-Varying Systems**

Systems following prescribed trajectories such as space launchers can be accurately modeled by explicitly time-varying nonlinear dynamic systems. The linearization about the reference trajectory then provides a finite horizon linear

time-varying system  $\mathbf{P}$  of the general form:

$$\begin{bmatrix} \dot{\mathbf{x}}(t) \\ \mathbf{y}(t) \end{bmatrix} = \begin{bmatrix} \mathbf{A}(t) & \mathbf{B}_d(t) & \mathbf{B}_u(t) \\ \mathbf{C}(t) & \mathbf{D}_d(t) & \mathbf{D}_u(t) \end{bmatrix} \begin{bmatrix} \mathbf{x}(t) \\ \mathbf{d}(t) \\ \mathbf{u}(t) \end{bmatrix}. \quad (1)$$

In (1),  $\mathbf{x}(t) \in \mathbb{R}^{n_x}$  is the state vector,  $\mathbf{u}(t) \in \mathbb{R}^{n_u}$  the input vector,  $\mathbf{d}(t) \in \mathbb{R}^{n_d}$  the disturbance vector, and  $\mathbf{y}(t) \in \mathbb{R}^{n_y}$  the output vector. The system matrices are locally bounded continuous functions of time  $t$ . They are compatible size-wise to the corresponding vectors, e.g.,  $\mathbf{A}(t) \in \mathbb{R}^{n_x \times n_x}$ . The explicit time dependence will be omitted regularly to shorten the notation.

A finite horizon LTV problem nullifies classic stability arguments as linear systems have no finite escape time [13] and system poles technically do not exist. Input-output norms present a more suitable metric for systems like launch vehicles, see, e.g., [14, 15]. “Unstable” dynamics are tolerable as long as no signal grows out of specified bounds, i.e. a specified norm gets too large. In principle, this characteristic can be exploited in the control design. The most common measure for the size of signals inside the LTV framework is the  $L_2[0, t_f]$  norm:

$$\|\mathbf{u}\|_{2[0, t_f]} = \left[ \int_0^{t_f} \mathbf{u}(t)^T \mathbf{u}(t) dt \right]^{\frac{1}{2}}. \quad (2)$$

In the course of the paper, the notation  $\mathbf{y} = [\mathbf{P}_d \ \mathbf{P}_u] \begin{bmatrix} \mathbf{u} \\ \mathbf{d} \end{bmatrix}$  is used to state the input-output map defined by the state space representation (1) for zero initial conditions. The performance of such a finite horizon LTV input-output map can be quantified by its finite horizon induced  $L_2[0, t_f]$  norm

$$\|\mathbf{P}\|_{2[0, t_f]} := \sup_{\substack{\begin{bmatrix} \mathbf{d} \\ \mathbf{u} \end{bmatrix} \in L_2[0, t_f], \begin{bmatrix} \mathbf{d} \\ \mathbf{u} \end{bmatrix} \neq \mathbf{0} \\ \mathbf{x}(0)=\mathbf{0}}} \frac{\|\mathbf{y}\|_{2[0, t_f]}}{\left\| \begin{bmatrix} \mathbf{d} \\ \mathbf{u} \end{bmatrix} \right\|_{2[0, t_f]}}, \quad (3)$$

where  $\mathbf{d} \in L_2[0, t_f]$  and  $\mathbf{u} \in L_2[0, t_f]$  imply  $\mathbf{y} \in L_2[0, t_f]$ . An upper bound on  $\|\mathbf{P}\|_{2[0, t_f]}$  is provided by a generalization of the Bounded Real Lemma (BRL) and can be found in [16].

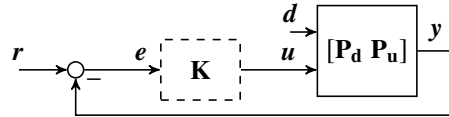


**Fig. 1 Standard unity feedback control loop**

In [8], the author’s proposed a novel observer-based induced  $L_2[0, t_f]$  controller synthesis procedure for LTV systems. Fig. 1 shows the standard unity feedback control loop with time-varying plant  $\mathbf{P}$  and time-varying controller  $\mathbf{K}$ .

Removing the controller from the interconnection yields the generalized plant  $\mathbf{G}$  with input  $\begin{bmatrix} w \\ u \end{bmatrix}$  and output  $\begin{bmatrix} z \\ e \end{bmatrix}$ . Here, the signals  $w$  and  $z$  represent measures for performance, e.g., the combination  $w = r$  and  $z = e$  measures the error in response to changes in the reference, see, e.g., [17]. The closed loop interconnection of  $\mathbf{G}$  and  $\mathbf{K}$  is denoted by the lower fractional transformation  $\mathcal{F}_1(\mathbf{G}, \mathbf{K})$ . The approach in [8] synthesizes an LTV controller  $\mathbf{K}$  minimizing the induced  $L_2[0, t_f]$  norm of  $\mathcal{F}_1(\mathbf{G}, \mathbf{K})$ :

$$\min_{\mathbf{K}} \|\mathcal{F}_1(\mathbf{G}, \mathbf{K})\|_{2[0, t_f]}. \quad (4)$$

where  $\mathbf{K}$  has the fixed structure:

$$\begin{bmatrix} \dot{\xi} \\ u \end{bmatrix} = \left[ \begin{array}{c|c} A(t) + B(t)F(t) + L(t)C(t) & L(t) \\ \hline F(t) & 0 \end{array} \right] \begin{bmatrix} \xi \\ e \end{bmatrix}, \quad (5)$$

In Eq. (5),  $L$  is a time-varying observer gain and  $F$  is a time-varying state feedback gain. The gains follow from the solution of two unidirectionally coupled Riccati differential equations provided in the following theorem under the assumption that the plant model (1) is strictly proper, i.e.,  $D_u = 0$  and  $D_d = 0$ , to simplify the notation. The theorem can be generalized to non-strictly proper plants at the cost of more complicated notation. However, usually engineering problems like space launcher can be accurately represented by strictly proper models, e.g., by including actuator dynamics in the model.

**Theorem 1 (Observer-Based Controller Synthesis)** *Consider an LTV system (1). There exists an observer-based controller  $\mathbf{K}$  defined by Eq. (5) such that  $\|\mathcal{F}_1(\mathbf{G}, \mathbf{K})\|_{2[0, t_f]} \leq \gamma$  if the following two conditions hold.*

- 1) *There exists a continuously differentiable, symmetric positive semi-definite matrix function  $Z(t)$ ,  $t \in [0, t_f]$  such that  $Z(0) = 0$  and*

$$\dot{Z} = AZ + ZA^T - ZC^T CZ + B_d B_d^T. \quad (6)$$

- 2) *There exists a continuously differentiable, symmetric positive semi-definite matrix function  $X(t)$ ,  $t \in [0, t_f]$  such that  $X(t_f) = 0$  and*

$$\dot{X} = -\bar{A}^T X - X \bar{A} + X \bar{T} X + C^T \bar{U} C, \quad (7)$$

$$\text{with } \bar{A} = A - \frac{1}{1-\gamma^2} Z C^T, \bar{T} = \frac{1}{1-\gamma^2} Z C^T C Z + B_u B_u^T, \text{ and } \bar{U} = \frac{\gamma^2}{1-\gamma^2} C^T C.$$

**Proof:** The proof is given in [8]. □

The solution of the RDE (6) provides the observer gain  $L = -Z C^T$ . In the same way, the solution of the RDE (7) guarantees the existence of a state feedback gain  $F = -B_u^T X$ . However, only the solution of the second RDE depends on  $\gamma$ . Thus, only RDE (7) has to be solved repeatedly in a bisection over  $\gamma$  to find the norm optimal controller. The

structured LTV synthesis provides the exact same induced  $L_2[0, t_f]$ -norm as the original LTV output feedback synthesis stated in, e.g., [9], [18], or [19]. However, the new approach is numerically more efficient due to the unidirectionally coupled RDEs. It further guarantees a fixed controller structure. The standard approaches require the solution of two bidirectionally coupled RDEs satisfying a spectral radius condition point-wise in time. Hence, two Riccati differential equations have to be solved repeatedly. The spectral radius condition can only be checked after integration and potentially renders a solution invalid which results in additional computational overhead. Moreover, the resulting controller has no particular structure.

### III. Space Launcher Control Design Problem

#### A. Launcher Model

The paper investigates the time-varying control design for an expandable launch vehicle (ELV). The ELV consists of three solid rocket motor (SRM) stages and a liquid-propelled upper module. The considered time segment spans 16.5 s to 103 s after lift-off. It covers the launcher’s atmospheric flight phase and concludes with the burnout of the first SRM.

##### 1. Nonlinear Rigid Body Dynamics

During the atmospheric ascent, the space launcher can be treated as perfectly symmetric, with fully decoupled pitch and yaw dynamics for small roll-rates [20, 21]. Thus, the pitch and yaw dynamics can be controlled by identical controllers. Given the flight segment’s overall duration and velocity regime, the earth can be assumed flat and non-rotating [20, 22] The control design considers the rigid body motion, first three bending modes and the tail-wags-dog effect caused by the nozzle inertia. Fuel sloshing is not considered as only the upper module uses liquid propellant. An illustration of the launcher’s pitch dynamics is given in Fig. 2. Forces are indicated by red and velocities by blue arrows. The launcher’s nonlinear equations of motion (EoM) are formulated with respect to its instantaneous center of gravity  $G$  in a body-reference coordinate system denoted by the subscript  $b$ . The  $x_b$ -axis is aligned with the launcher’s symmetry axis and is defined positive in the direction of forward travel. The  $z_b$ -axis points downward, forming a right-hand system

with the  $y_b$ -axis. The launcher's nonlinear EoM in the pitch plane are described by:

$$\begin{aligned}
\ddot{\theta}_b(t) &= \frac{\sum M_y(Ma, \alpha, h, t)}{J_{yy}(t, m)} - \dot{\theta}_b \frac{\dot{J}_{yy}(m, t)}{J_{yy}(m, t)} \\
&= \frac{N(Ma, \alpha, h, t)l_{GP}(Ma, m, t)}{J_{yy}(t, m)} - \dot{\theta}_b \frac{\dot{J}_{yy}(m, t)}{J_{yy}(m, t)} - \frac{T(t)l_{CG}(t, m)}{J_{yy}(t, m)} \sin \delta_{TVC}(t) + \frac{M_{N,y}(m, t)}{J_{yy}(m, t)} \\
\ddot{x}_b(t) &= \frac{\sum F_x(Ma, \alpha, h, t)}{m(t)} - \dot{\theta}_b(t)\dot{z}_b(t) \\
&= \frac{T(t) \cos \delta_{TVC}(t) - A(Ma, \alpha, h, t)}{m(t)} - g_0(h) \sin \theta_b(t) - \dot{\theta}_b(t)\dot{z}_b(t) \\
\ddot{z}_b(t) &= \frac{\sum F_z(Ma, \alpha, h, t)}{m(t)} - \dot{\theta}_b(t)\dot{x}_b(t) \\
&= -\frac{N(Ma, \alpha, h, t)}{m(t)} - \frac{T(t)}{m(t)} \sin \delta_{TVC}(t) + g_0(h) \cos \theta_b(t) + \frac{F_{N,z}(t)}{m(t)} - \dot{\theta}_b(t)\dot{x}_b(t) \\
\dot{m}(t) &= -\frac{1}{v_{ex}}(t)T(t).
\end{aligned} \tag{8}$$

In Eq. (8),  $\sum M_y$  is the sum of moments around the pitch axis formulated with respect to the center of gravity  $G$ . The sum of forces in  $x_b$  and  $z_b$  direction are denoted by  $\sum F_x$  and  $\sum F_z$ , respectively. The launcher's pitch angle corresponds to the angle between the  $x_b$  axis and the local horizon. It is denoted  $\theta_b$ . The axial and normal accelerations are denoted  $\ddot{x}_b$  and  $\ddot{z}_b$ . Finally,  $A$  and  $N$  are the axial and normal aerodynamic forces acting on the launcher's center of pressure  $P$ .

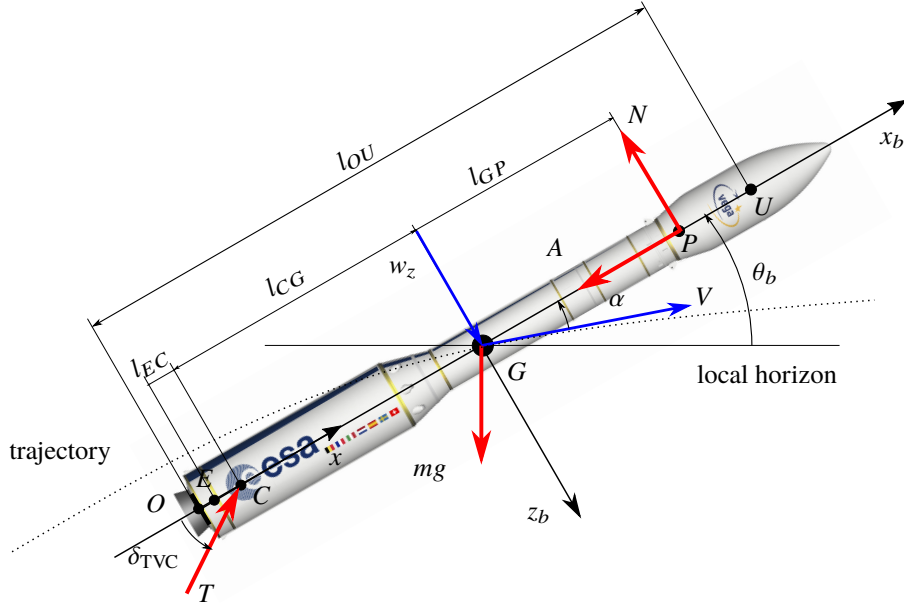


**Fig. 2** Expandable launch vehicle in body fixed reference frame

They are defined by

$$\begin{aligned} A(Ma, \alpha, h, t) &= \bar{q}(h, t) S_{\text{ref}} C_A(\alpha, Ma) \\ N(Ma, \alpha, h, t) &= \bar{q}(h, t) S_{\text{ref}} C_N(\alpha, Ma), \end{aligned} \quad (9)$$

with the dynamic pressure  $\bar{q}(h, t) = 0.5\rho(h)V^2(t)$ , reference area  $S_{\text{ref}}$  and aerodynamic force coefficients  $C_A$  and  $C_N$ . These coefficients dependent nonlinearly on the Mach number  $Ma$  and the angle of attack. The variable  $V$  is the absolute aerodynamic velocity of the ELV and is referred to as the launch vehicle airspeed. The density of the air  $\rho$  is calculated according to the international standard atmosphere (ISA) [23]. The aerodynamic forces are expressed in body axes rather than in a coordinate system attached to the aerodynamic velocity. Here, the axial and normal forces are defined in the negative axis directions. Thus,  $A$  acts in negative  $x_b$  direction and  $N$  acts in negative  $z_b$  direction. In Eq. (9), the angle of attack is approximated as

$$\alpha(t) \approx \frac{\dot{z}_b(t) - w_z(t)}{\dot{x}_b(t)}, \quad (10)$$

where  $w_z$  is the external wind disturbance aligned with the  $z_b$ -axis.

The launcher's thrust  $T$  acts at the nozzle reference point  $C$ . It can be rotated by the angle  $\delta_{\text{TVC}}$  using the thrust vector control (TVC) system. Due to the characteristics of the solid rocket motor, the thrust follows a predefined time profile after ignition. Hence, the thrust at a certain point in time is given by:

$$T(t) = v_{\text{ex}}(t)\dot{m}_{\text{ex}}(t), \quad (11)$$

where  $v_{\text{ex}}$  is the exhaust velocity and  $\dot{m}_{\text{ex}}$  the exhaust mass flow of the engine. The thrust profile (11) directly relates to the launcher mass  $m$  through  $m_{\text{ex}}$ :

$$m(t) = m_0 - \int_0^{t_f} \dot{m}_{\text{ex}} dt = m_0 - \int_0^{t_f} \frac{T(t)}{v_{\text{ex}}(t)} dt. \quad (12)$$

The overall moment of inertia  $J_{yy}$  is defined with respect to the instantaneous center of gravity  $G$  and depends directly on the launcher's momentary mass. The same is true for the center of gravity itself. The altitude-dependent gravitational acceleration  $g_0(h)$  is calculated based on the world geodetic system 84 (WGS 84) [24] with a launch site close to the equator. Moving the nozzle causes a reactive force and moment acting through the gimbal mechanism. This is the so-called tail-wags-dog effect. The force and moment depend on the nozzle mass  $m_N$ , nozzle inertia  $J_N$ , and

angular acceleration  $\ddot{\delta}_{\text{TVC}}$ :

$$\begin{aligned} F_{N,z} &= -m_N l_{EC} \ddot{\delta}_{\text{TVC}} \\ M_{N,y} &= -(m_N l_{EC} l_{CG}(m,t) + J_N) \ddot{\delta}_{\text{TVC}} \end{aligned} \quad (13)$$

The distance between nozzle reference point and the nozzle's center of mass  $E$  is denoted  $l_{EC}$ .

A second-order transfer function with unit steady state gain  $k_{\text{TVC}}$ , natural frequency  $\omega_{\text{TVC}} = 50$  rad/s, and damping ratio  $\zeta_{\text{TVC}} = 0.7$  is used to model the dynamics of the thrust vector control system. The TVC dynamics are connected to the launch vehicle rigid body dynamics via  $\delta_{\text{TVC}}$  and  $\ddot{\delta}_{\text{TVC}}$  to model the tail-wags-dog effect given in Eq. (13). The commanded TVC deflection  $\delta_{\text{TVC,c}}$  is the sole control input. The TVC has a maximum deflection angle of  $\pm 5.5$  deg and maximum deflection rate of  $\pm 10.0$  deg/s.

## 2. Flexible Body Dynamics

The ELV's elastic deflection at any point along the vehicle's symmetry axis is given by:

$$\epsilon(x,t) = \sum_{i=1}^{\infty} q_i(t) \phi_i(x), \quad (14)$$

where  $x$  is the distance from the launcher geometry reference point  $O$  along the ELV's longitudinal axis as depicted in Fig. 2. The variable  $\phi_i$  denotes the mass normalized  $i$ -th spatial mode shape in the pitch plane, and  $q_i$  the generalized coordinate of the  $i$ -th mode which satisfies:

$$\ddot{q}_i + 2\zeta_i \omega_i(m) \dot{q}_i + \omega_i^2(m) q_i = Q_i. \quad (15)$$

The mode frequencies  $\omega_i$  are functions of the launcher mass  $m$ . The generalized force  $Q_i$  associated with the  $i$ -th mode is a function of the moments and normal forces acting on the launch vehicle. For the given launch vehicle, the bending modes are mainly excited by the rocket engine. Assuming only first-order effects the generalized forces can be written as:

$$Q_i = -(T \delta_{\text{TVC}} + m_N l_{EC} \ddot{\delta}_{\text{TVC}}) \phi_i(l_{OC}) + J_N \ddot{\delta}_{\text{TVC}} \frac{\partial \phi(l_{OC})}{\partial x}. \quad (16)$$

The length  $l_{OC}$  denotes the distance of the launcher geometric frame's origin  $O$  to the nozzle reference point  $C$ . The flexible modes have a direct influence on the control system as they directly impact measurements provided by the inertial measurement unit (IMU). Control feedback measurements include  $\theta_{\text{IMU}}$ ,  $\dot{\theta}_{\text{IMU}}$ , and  $\dot{z}_{\text{IMU}}$  which are the superimposed

rigid body motion and elastic deformation at the IMU location  $l_{OU}$ :

$$\begin{aligned}
\theta_{\text{IMU}} &= \theta_b - \left. \frac{\partial \epsilon}{\partial x} \right|_{x=l_{OU}} = \theta_b - \sum_i q_i \left. \frac{\partial \phi_i}{\partial x} \right|_{x=l_{OU}} = \theta_b - \sum_i q_i(t) \sigma_i(l_{OU}) \\
\dot{\theta}_{\text{IMU}} &= \dot{\theta}_b - \sum_i \dot{q}_i(t) \sigma_i(l_{OU}) \\
\dot{z}_{\text{IMU}} &= \dot{z}_b - \dot{\theta}_b l_{GU} - \sum_i \dot{q}_i(t) \phi_i(l_{OU})
\end{aligned} \tag{17}$$

The variable  $\sigma_i = \frac{\partial \phi_i}{\partial x}$  denotes the local rotation of the  $i$ -th mode.

### 3. Wind Model

The vertical component of a representative wind profile for the considered trajectory from an equatorial launch side can be found in [25]. This vertical wind profile is estimated from the post-flight analysis of the Vega space launcher flight VV05. Fig. 3 depicts the wind profile (—). This wind signal can be decomposed into a steady and a turbulent component. Fig. 3 shows the steady component (⋯⋯). It builds up and decays similarly to the original VV05 profile. The constant value in-between equals the calculated mean value of the VV05 profile. The turbulent wind component has a varying maximum amplitude along the flight which decays to a value of zero after 65 s. Steady wind fields can be estimated with good accuracy pre-flight. Turbulence is of stochastic nature. Thus, it has to be treated as such in the controller evaluation to verify performance under non-nominal conditions. Hence, a turbulence wind filter is designed based on the representative wind profile's turbulent component [25]. The design approach originates from the classical Dryden wind model described in, e.g., [26], which is based on the power spectral density of the turbulence. In a first step, the deviation from the mean wind signal  $w_z$  (i.e., the wind velocity (—) minus the steady profile (⋯⋯) in Fig. 3) is divided into five second long time segments spanning from 16.5 s to 66.5 s. Based on the wind profile in Fig. 3, zero wind is assumed for times later than 65s after lift-off. Note that after 65 s the launcher has reached such a high altitude that wind is no longer a factor. Given the time history of the reference wind signal  $w_z$ , the power spectral density (PSD)  $\Omega_{w_z,k}$  of a segment  $k$  is calculated by

$$\Omega_{w_z,k}(\omega) = \lim_{t_{f,k} \rightarrow \infty} \frac{2}{\pi} \frac{1}{t_{f,k}} \left| \int_0^{t_{f,k}} w_{z,k}(t) e^{-j\omega t} dt \right|^2, \tag{18}$$

with  $t_{f,k}$  defining the time span of the segment, where  $w_{z,k}(t)$  has been truncated to have zero value outside the range 0 to  $t_{f,k}$ . Hence, the PSD of a signal is determined by the average squared of its Fourier transform. In the present paper, the internal Matlab function `fft` is applied for this purpose using a sampling rate of 100 Hz. This calculation is repeated for all segments  $n$  of the wind profile. In a second step, for each time segment, a transfer function upper bounding the respective  $|\Omega_{w_z,k}|$  is calculated. For this purpose, the internal Matlab function `fitmagfrd` is applied, which determines

a minimum phase transfer function using log-Chebyshev magnitude design. The fitted transfer functions are then transformed into consistent state-space models. In the third and final step, an LTV representation  $\mathbf{G}_{w_z, \text{LTV}}$  of the wind filter is calculated by linearly interpolating the system matrices' coefficients over the analysis horizon. By definition, this filter shapes a white noise input  $n_w(t)$  with a power spectral density  $\Phi_{n_w} = 1$  into a continuous turbulence signal with the same time-dependent/altitude-dependent spectral characteristics as the original signal  $w_z$ . Here, the Simulink internal band-limited white noise block is used to generate  $n_w(t)$ . Fig. 3 shows the envelope of 1000 wind signals (—) created by the calculated turbulence filter superimposed with the steady wind profile. The comparison of two selected signals (—) with the original VV05 signal shows a good qualitative match. The generated wind signals are used for the control performance evaluation in Section V. Note that the wind axes are aligned with the body-referenced coordinate system. This assumption follows common definitions of certified wind models for higher altitudes, see, e.g., [26]. Only vertical wind is considered due to its immediate impact on the launcher's angle of attack.

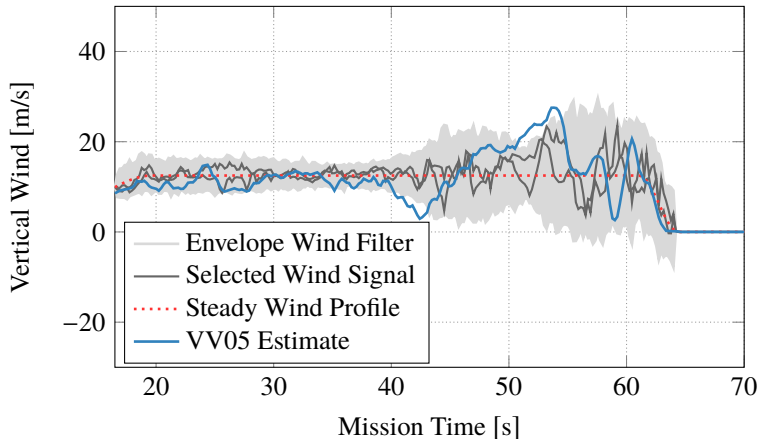


**Fig. 3 Vertical wind profiles**

## B. Atmospheric Ascent Problem

The atmospheric flight phase poses the most challenging launch segment. A multitude of performance requirements are imposed on the launch system, while it accelerates through the densest atmosphere layers.

### 1. Trajectory Calculation and Linearization

The nominal trajectory of a space launcher through the earth's atmosphere must fulfill multiple requirements. The trajectory shall maximize the acceleration in the longitudinal axis of the launcher with the least amount of fuel possible to reduce the necessary lift-off mass. Hence, the TVC deflection shall be approximately zero during the ascent. At the same time, the static aerodynamic loads in the lateral direction shall be minimized, i.e., the angle of attack shall be approximately zero. A maneuver called gravity turn fulfills both requirements [27, 28]. Under the constraint that only a velocity component in  $x_b$ -direction exists, i.e.,  $\alpha = 0$ , the normal acceleration due to curvature of the launcher trajectory

and the gravitational acceleration on the launcher must compensate each other. The balance of both forces leads to the set of equations:

$$\begin{aligned} \dot{h} &= \dot{x}_b \sin \theta_b & \dot{D} &= \dot{x}_b \cos \theta_b \\ \ddot{x}_b &= \frac{T - A}{m} - g_0 \sin \theta_b & \dot{\theta}_b &= -\frac{g_0}{\dot{x}_b} \cos \theta_b \end{aligned} \quad (19)$$

derived from the launcher's equations of motion (8). In Eq. (19),  $h$  is the altitude and  $D$  is the downrange distance. Solving Eq. (19) for a given  $h_0$ ,  $\theta_0$ ,  $\dot{x}_{b_0}$  and  $D_0$  provides a so-called pitch program for the launcher. Fig. 4 shows the reference pitch angle  $\theta_{\text{ref}}$ , pitch rate  $\dot{\theta}_{\text{ref}}$ , velocity  $V_{\text{ref}}$ , and altitude  $h_{\text{ref}}$  for the considered kick-angle  $\theta_0$  and thrust profile. This ascent profile results in  $\alpha \approx 0$  and  $\delta_{\text{TVC}} \approx 0$  for nominal launcher dynamics and no external disturbances. A control

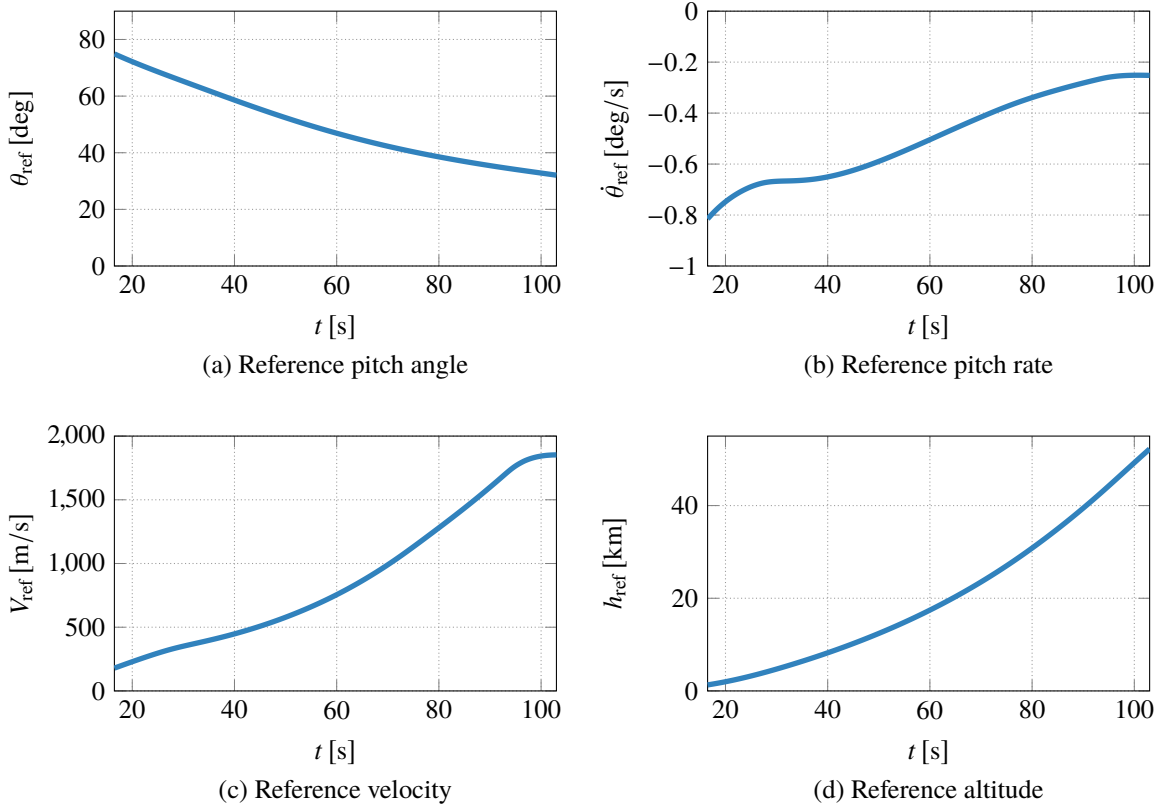


**Fig. 4 Reference gravity turn trajectory**

system is required to stabilize the inherently unstable launcher dynamics while tracking the pitch program.

The controller synthesis from Section II requires an LTV representation of the ELV along the calculated gravity turn trajectory. This LTV model is calculated by numerically linearizing the nonlinear dynamics in Eq. (8) over the considered trajectory segment spanning 16.5 s to 103 s after lift-off using a step size of 0.5 s. The result is a finite horizon LTV system  $\mathbf{P}$  as defined in Eq. (1). The state vector including the linear actuator dynamics is  $\mathbf{x} = [\Delta\theta_b, \Delta\dot{\theta}_b, \Delta\dot{z}_b, \Delta\dot{x}_b, \Delta q_i, \Delta\dot{q}_i, \Delta\delta_{\text{TVC}}, \Delta\dot{\delta}_{\text{TVC}}]^T$ , the disturbance vector is  $d = \Delta w_z$ , the input vector is  $u = \Delta\delta_{\text{TVC},c}$ ,

and the output vector is  $\mathbf{y} = [\Delta\theta_{\text{IMU}}, \Delta\dot{\theta}_{\text{IMU}}, \Delta\dot{z}_{\text{IMU}}]^T$ . The symbol  $\Delta$  refers to the deviation from the reference value on the design trajectory.

## 2. Control Objectives

The control design considers the time horizon from 16.5 s to 103 s after lift-off; the start and end point of the gravity turn maneuver. The first control objective is tracking performance under external disturbances such as atmospheric turbulence. The launcher must accurately follow the reference trajectory, i.e.  $\theta_{\text{ref}}$ , ideally with zero error. The response time to wind disturbances must be adequately fast, which requires sufficient controller bandwidth. Additionally, the transient response shall be constrained regarding maximum overshoot and maximum  $\dot{\theta}$ . Before engine burnout, i.e., shortly before the stage separation is triggered, the absolute value of the pitch error must be smaller than 0.5 deg. At stage separation a maximum absolute pitch rate error of 0.5 deg/s is allowed. These values shall guarantee a clean stage separation. Larger values (up to 1 deg absolute pitch error and 5 deg/s absolute pitch rate error) are acceptable before stage separation, e.g., for load relief purposes.

The second control objective considers the reduction of aerodynamic loads on the launcher caused by wind disturbances and trajectory perturbations. This objective is usually given in form of the maximum absolute value of the static aerodynamic load  $\bar{q}\alpha$ , i.e., the product of momentary angle of attack and dynamic pressure. Fig. 5 shows the  $\bar{q}\alpha$  bound of the considered launch vehicle over its Mach number. Load reduction can only be achieved by either turning into the wind or drifting with the wind. Both approaches lead to a vertical drift away from the trajectory. Another contributor to aerodynamic loads and the drift of the launch vehicle are uncertainties in thrust and mass. These lead to a violation of the gravity turn equations (19) for the provided open-loop guidance profile  $\theta_{\text{ref}}$ . The result is a build-up of  $\alpha$  as well as a continuously increasing deviation from the design trajectory.

Limiting the drift away from the nominal trajectory poses the third control requirement. Large deviations from the trajectory must be avoided as these are not correctable in later flight phases. At the moment of stage separation, the drift is limited to  $\pm 20$  m/s for a safe separation. For load relief purposes, larger values are acceptable in the high dynamic pressure region.

The last two control objectives concern the thrust vector control. First, the demanded TVC actuation shall neither reach its deflection or rate limit ( $\pm 5.5$  deg and  $\pm 10$  deg/s, respectively) nor exceed the actuator bandwidth limit of 50 rad/s. The second TVC objective concerns the required fuel reserves, and therefore directly the cost-critical lift-off mass of the launcher. In order to maximize forward acceleration for a given thrust profile, the launcher shall not exceed a given cumulated commanded thrust deflection (the so-called TVC consumption quantified by  $\int_0^{t_f} |\delta_{\text{TVC}}| dt$ ). A typical value for this type of launcher and trajectory segment is 250 deg s. Tab. 1 summarizes the discussed performance requirements of the considered space launcher.

In general, tracking, drift, and load relief objectives contradict each other, as tracking a given pitch angle and limiting

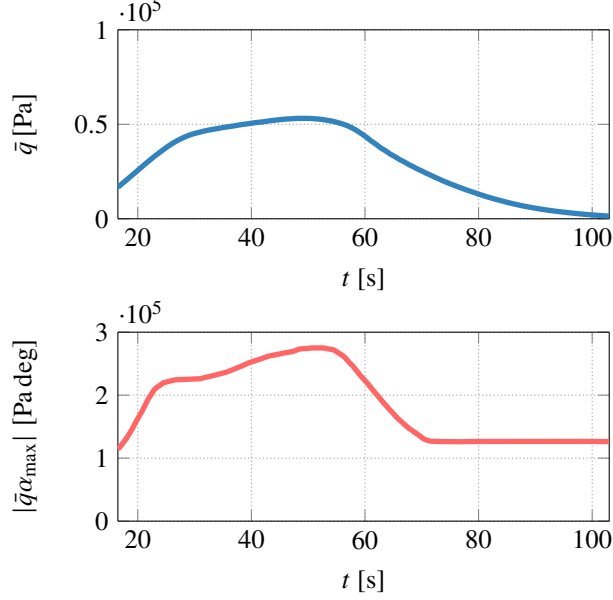


**Fig. 5** Dynamic pressure  $\bar{q}$  along the trajectory and corresponding  $|\bar{q}\alpha_{\max}|$ .

**Table 1** Launch vehicle performance requirements

Requirement	Metric	Constraint
Load Performance	$ \bar{q}\alpha $	$< \bar{q}\alpha$ boundary
Tracking Performance	$ \Delta\theta_{\text{IMU}} $	$< 0.5$ deg
	$ \Delta\dot{\theta}_{\text{IMU}} $	$< 0.5$ deg/s
Drift Performance	$ \dot{z}_{\text{IMU}} $	$< 20$ m/s
	$ \delta_{\text{TVC}} $	$< 5.5$ deg
Actuation	$ \dot{\delta}_{\text{TVC}} $	$< 10$ deg/s
	$\int_0^{t_f}  \delta_{\text{TVC}}  dt$	$< 250$ deg s

drift under wind disturbance results in a significant aerodynamic load build-up. Tight pitch control in the region of high dynamic pressure with large expected disturbances can result in a loss of the launch vehicle if  $\bar{q}\alpha_{\max}$  is exceeded. Vice versa, minimizing  $\bar{q}\alpha$  by allowing the launcher to drift with the wind results in a deviation from the trajectory too large to correct and, thus, likewise in mission failure. Also, reducing the launcher's drift rate requires a pitch motion, which opposes pitch tracking. In summary, the control objectives for launch vehicles require a trade-off between trajectory tracking and load alleviation. This trade-off is imposed by the dynamic pressure  $\bar{q}$  and expected wind disturbances, i.e., favoring load alleviation in the  $\bar{q}_{\max}$  region and tracking later in the flight.

The time-varying launcher dynamics further complicate the control problem. Important dynamic properties of the launcher can be characterized by the launcher specific parameters  $a_6 = \frac{\partial N}{\partial \alpha}(t) \frac{l_{GP}}{J_{yy}}$  and  $k_1 = \frac{T_{CG}}{J_{yy}}$  (see, e.g., [21]). The variable  $\frac{\partial N}{\partial \alpha}(t)$  denotes the partial derivative of  $N$  along the trajectory following from the numerical linearization.

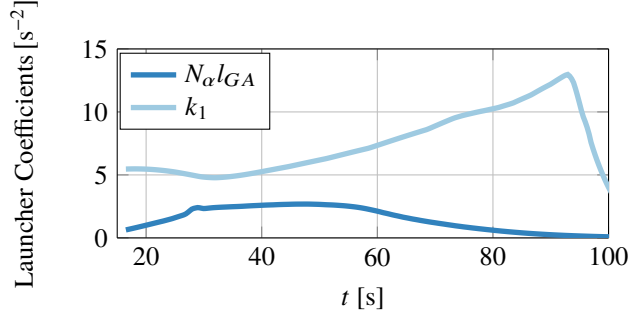


**Fig. 6 Launcher specific moment coefficients along the trajectory.**

The parameter  $a_6$  is a measure for the time to double of the pitch angle. Larger values of  $a_6$  indicate faster times posing a more difficult control problem. Thus, there exists a time-varying minimum closed loop bandwidth threshold along the ascent. The parameter  $k_1$  quantifies the launcher’s ability to counteract destabilizing aerodynamic moments by deflecting the TVC. A larger value relates to higher control authority. Fig. 6 depicts the two parameters’ rapidly changing values along the ascent showcasing the time-varying nature of the problem. Smaller ratios of  $k_1/a_6$  pose a harder pitch tracking problem. The smallest ratios occur in the high dynamic pressure region rendering the trade-off between pitch tracking and load relief even more delicate. Hence, time-varying control is beneficial to not only account for the time-dependent control objectives, but also the time-varying launcher dynamics.

## IV. Structured Linear Time-Varying Launcher Control Design

### A. Converting Control Objectives to Weighting and Tuning

An apparent and transparent translation of the time-varying control objectives to tuning rules is required for rapid and traceable control designs. Hence, the proposed design uses a specifically parameterized four-block mixed sensitivity formulation proposed in [10, 29]. Fig. 7 shows a graphical representation of the closed loop synthesis structure. It

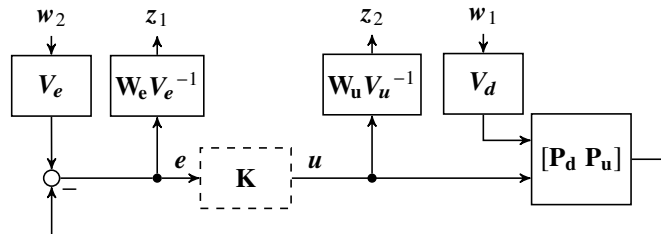


**Fig. 7 Weighted four-block mixed sensitivity problem.**

characterizes the control objectives in form of an induced  $L_2[0, t_f]$  norm optimization of the weighted closed loop with

the associated controller synthesis problem:

$$\min_K \left\| \begin{bmatrix} \mathbf{W}_e \mathbf{V}_e^{-1} & 0 \\ 0 & \mathbf{W}_u \mathbf{V}_u^{-1} \end{bmatrix} \begin{bmatrix} -\mathbf{S} \mathbf{P}_d & \mathbf{S} \\ -\mathbf{K} \mathbf{S} \mathbf{P}_d & \mathbf{K} \mathbf{S} \end{bmatrix} \begin{bmatrix} \mathbf{V}_d & 0 \\ 0 & \mathbf{V}_e \end{bmatrix} \right\|_{2[0, t_f]} . \quad (20)$$

The LTV observer-based control synthesis framework introduced in Section II can be easily applied to solve the optimization problem. In (20),  $\mathbf{S} = (\mathbf{I} + \mathbf{P}_u \mathbf{K})^{-1}$  denotes the output sensitivity function [30]. It relates reference inputs to control errors. Accordingly,  $\mathbf{K} \mathbf{S}$  relates reference inputs to control effort. The disturbance sensitivity  $\mathbf{S} \mathbf{P}_d$  corresponds to the impact of disturbances on the closed-loop.

The time-varying dynamic weighting filters  $\mathbf{W}_u$  and  $\mathbf{W}_e$  have the state space realization:

$$\begin{bmatrix} \dot{\xi}_e \\ z_1 \end{bmatrix} = \begin{bmatrix} 0 & \mathbf{B}_{\mathbf{W}_e}(t) \\ \mathbf{C}_{\mathbf{W}_e}(t) & \mathbf{D}_{\mathbf{W}_e}(t) \end{bmatrix} \begin{bmatrix} \xi_e \\ \tilde{e} \end{bmatrix} \quad (21a)$$

$$\begin{bmatrix} \dot{\xi}_u \\ z_2 \end{bmatrix} = \begin{bmatrix} \mathbf{A}_{\mathbf{W}_u}(t) & \mathbf{B}_{\mathbf{W}_u}(t) \\ \mathbf{C}_{\mathbf{W}_u}(t) & \mathbf{D}_{\mathbf{W}_u}(t) \end{bmatrix} \begin{bmatrix} \xi_u \\ \tilde{u} \end{bmatrix} . \quad (21b)$$

Based on the control objectives (see Tab. 1) and the expected disturbances, the dynamic weights  $\mathbf{W}_e$  and  $\mathbf{W}_u$ , as well as memoryless scaling matrices  $\mathbf{V}_e$ ,  $\mathbf{V}_u$ , and  $\mathbf{V}_d$  are selected. The former represent principle design requirements such as bandwidths and roll-offs. These requirements are mainly imposed by the plant dynamics. Once identified, they usually remain unchanged and are not part of the iterative tuning process. The memoryless weights are then used for the quantitative tuning of the controller to address, e.g., allowable control efforts or errors. Time-varying objectives increase the tuning complexity. Hence, such an intuitive parameterization which also includes “non-tuneable” elements is beneficial.

The weighting filter  $\mathbf{W}_e$  affects the disturbance sensitivity. A high gain in  $\mathbf{W}_e$  enforces a sensitivity reduction and specifies tracking and disturbance rejection capabilities. The weight  $\mathbf{W}_{e_\theta}$  in the  $\theta_{\text{IMU}}$  channel is selected with integral behavior up to 3.5 rad/s and a magnitude of 0.5 beyond for times up to 40 s into the ascent. Doing so, sensitivity is reduced up to the desired closed-loop bandwidth  $\omega_{\text{bw}}$  and peak sensitivity beyond this frequency is limited to a factor of  $1/0.5 = 2$ . The bandwidth is increased to a value of 4.0 rad/s between 50 s and 80 s until it reaches a maximum of 5.5 rad/s at stage-separation. The design aims for a closed-loop bandwidth, which is at least two-times faster than the momentary unstable pitch pole along the trajectory (visualized by the red line in the *Bandwidth* plot in Fig. 8). It also seeks to separate the closed loop bandwidth by a factor of at least nine from the TVC’s bandwidth. The first increase in

bandwidth accounts for the increasing wind disturbance amplitudes (see Fig. 3). The final increase targets the required tracking performance before stage separation. Faster control is necessary to keep pitch deviations and thus required control moments small as the available control moment reduces rapidly before burnout. The explicit time-varying parameterization of  $\mathbf{W}_{e_\theta}$  used for the synthesis is:

$$\begin{bmatrix} \dot{\xi}_{e_\theta} \\ z_{1_\theta} \end{bmatrix} = \begin{bmatrix} 0 & | & 0.5 \\ \hline 2\omega_{\text{bw}}(t)\sqrt{(1-0.5^2)} & | & 0.5 \end{bmatrix} \begin{bmatrix} \xi_{e_\theta} \\ \tilde{e}_\theta \end{bmatrix}. \quad (22)$$

The close loop bandwidth  $\omega_{\text{bw}}$  is provided in Tab. 2. To guarantee smoothness, piecewise cubic Hermite interpolating polynomials (PCHIPs) are used to calculate the points in-between the grid points. A frequency-independent constant weighting is chosen for the remaining feedback signals, namely  $\dot{\theta}_{\text{IMU}}$  ( $W_{e_\theta} = 0.5$ ) and  $\dot{z}_{\text{IMU}}$  ( $W_{e_z} = 0.5$ ). The rationale is again to limit the peak sensitivity to less than  $1/0.5 = 2$ . The weighting filter  $\mathbf{W}_u$  determines the control sensitivity and represents the actuator limitations as well as robustness requirements. It is selected with unit gain up to a roll-off frequency  $\omega_{\text{wo}}$  of 25 rad/s, i.e., half the thrust vectoring control bandwidth and as high as the first flexible modes slowest natural frequency. Beyond 25 rad/s, differentiating behavior is selected to enforce controller roll-off. The explicit parameterization of  $\mathbf{W}_u$  used for the controller synthesis is:

$$\begin{bmatrix} \dot{\xi}_u \\ z_2 \end{bmatrix} = \begin{bmatrix} -100\omega_{\text{ro}} & | & 100\omega_{\text{ro}} \\ \hline -99 & | & 100 \end{bmatrix} \begin{bmatrix} \xi_u \\ \tilde{u} \end{bmatrix}. \quad (23)$$

After the dynamic weights are set, the time-varying scaling factors  $\mathbf{V}$  are selected, which are based on the control objectives in Section III.B.2. The scaling factors  $\mathbf{V}_e$  and  $\mathbf{V}_u$  trade off tracking accuracy and control effort. They can be selected based on the maximum allowable errors ( $V_e$ ) and maximum allowable inputs ( $V_u$ ) at specific trajectory segments. The value of  $V_e$  is primarily based on the pitch tracking requirements along the trajectory. At the beginning of the gravity turn, load relief is prioritized over pitch tracking and  $V_e$  is chosen to 0.75 deg in the  $\theta_{\text{IMU}}$  channel ( $V_{e_\theta}$ ). The value is reduced to 0.5 deg at 50 s. The reduction at this time avoids large pitch angles where the disturbances are expected large and the combination of instability and controllability is least favorable (see Fig. 6). This value also represents the pitch angle requirement at stage-separation. Accordingly,  $V_e$  in the  $\dot{\theta}_{\text{IMU}}$  channel ( $V_{e_\dot{\theta}}$ ) starts high and is gradually reduced to slow down the transient behavior along the ascent. The final value of 0.5 deg/s equals the pitch rate requirement at stage separation. A constant value of 15 m/s is chosen for the weight  $V_{e_z}$ , which also equals the drift rate requirement at state separation. It reduces the drift from the reference trajectory without overly negative impact on load alleviation.

The value  $V_u$  assigns the available control action to counteract the previously specified maximum errors. The

TVC saturation limit directly provides an upper bound for its maximum value.  $V_u$  also addresses the consumption requirement. For the considered launcher, a value of 2.5 deg in the high pressure region is chosen and 3.0 deg elsewhere. This choice also reduces the control effort in the high pressure region for load alleviation purposes. Finally, the ratio  $V_e/V_d$  determines the trade-off between tracking performance and disturbance rejection. Hence, disturbance rejection is favored in the high dynamic pressure range. The selected values for  $V_d$  are motivated by the expected gusts.

**Table 2 Values of the weights along the trajectory**

Tuning Parameter	16.5 s	30 s	40 s	50 s	60 s	80 s	103 s
$\omega_{bw}$ [rad/s]	3.5	3.5	3.5	4.0	4.0	4.0	5.5
$V_{e_z}$ [m/s]	15	15	15	15	15	15	15
$V_{e_\theta}$ [deg]	0.75	0.75	0.5	0.5	0.5	0.5	0.5
$V_{e_{\dot{\theta}}}$ [deg/s]	3.5	3.5	3.5	3.5	3.5	2.0	0.5
$V_u$ [deg]	3.0	3.0	3.0	3.5	3.5	3.5	4.0
$V_d$ [m/s]	10	10	10	10	5	5	5

Tab. 2 summarizes the numerical values chosen for the elements of  $V_e$ ,  $V_u$ , and  $V_d$ . For smoothness, PCHIPs are again used to calculate the points in-between the grid points. Fig. 8 depicts the scaling factors along the trajectory.

## B. LTV Controller Synthesis and Implementation

Using the weights provided in Tab. 2 and the LTV representation of the launcher (see Section III.B.1) the structured LTV controller is synthesized. First, the observer gain  $L$  is calculated by solving a scaled version of the RDE (6). This scaled RDE can be readily derived following the step by step explanations in [29]. It is solved using the Matlab solver ODE15s [31], suitable for stiff differential equations, a typical property of RDEs, see e.g. [32]. The solution takes 2 s on a standard desktop PC. Next, the state feedback synthesis is conducted using  $L$  in an augmented version of the state feedback RDE (7). Matlab's ODE15s solves this RDE repeatedly in a bisection over  $\gamma$ . The bisection calculates the minimal feasible  $\gamma$  of 3.75 in 239 s. This  $\gamma$  value is the optimal solution of the output feedback problem (20). In total, the controller synthesis requires approximately 241 s.

Finally, the structured finite horizon LTV controller is assembled from the feasible solutions of the RDEs, the plant and weighting filter state space matrices and static weights. Fig. 9 shows the controller's fixed, traceable, and easily implementable structure. It consists of a dynamic part whose outputs are fed into the static state feedback controller. The controller dynamics consist of three elements with clear interpretations. The first element, *Integral Augmentation*, provides tracking properties with zero steady state error.  $W_e$  contains only integral dynamics and can be interpreted as an integral (I) controller. The second dynamic part is the *Luenberger Observer*. The third dynamic element, namely

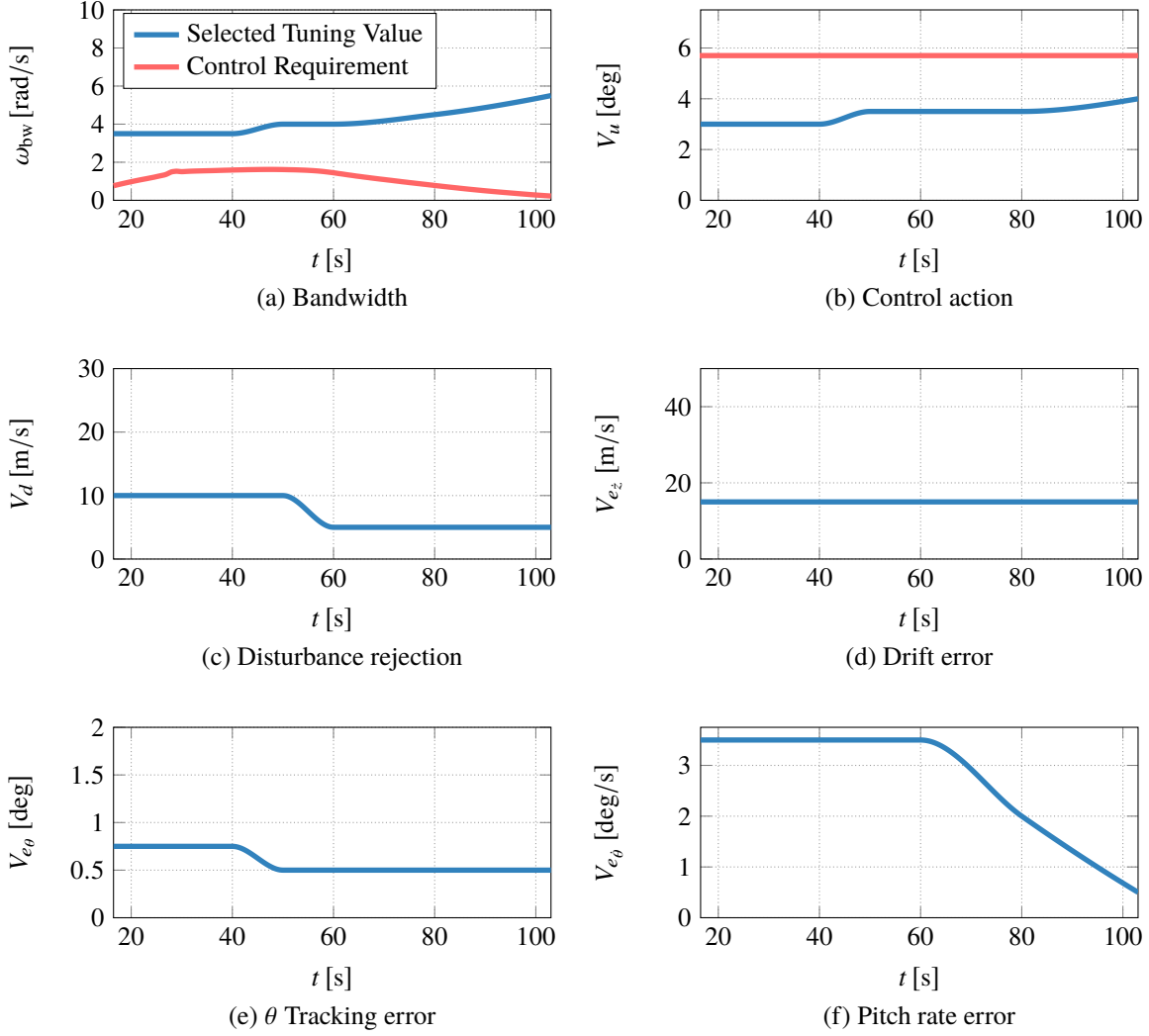


**Fig. 8 Tuning parameters and control requirements along the trajectory**

*Roll-Off Augmentation*, provides the additional user-specified control roll-off for frequencies above 25 rad/s providing extra robustness for high frequencies. The integrator in the integral augmentation appears explicitly. This property can be exploited in the implementation, e.g., to include simple anti-wind-up compensation [33].

The low amount of time for synthesis and the transparent weighting scheme allow for a fast tuning process. Another advantage of the structured LTV synthesis is that it allows significantly denser grids and higher order systems compared to classic LTV output feedback synthesis and LPV approaches for launcher control, see e.g. [5]. Thus, significantly more accurate representations of the launcher dynamics are possible in the synthesis. This is especially important for the flexible dynamics, which can be easily included into the control design. The proposed controller synthesis hence directly includes flex-mode attenuation and stabilization. Therefore, high-order bending filters can be avoided. Such bending filters can easily be of 14-th order resulting in very high order control systems. In comparison, the present controller has fourteen states in total. Moreover, these bending filters have to be tediously tuned by hand requiring expert knowledge.

Note that no wind model is included into the synthesis for multiple reasons. First, the wind model would be estimated by the observer and increase the controller order. Moreover, the influence on the closed loop performance, i.e., disturbance attenuation, is already covered by the requirements on sensitivity.

Although, the controller is synthesized with a dependence on time, time after lift-off does not present the most suitable scheduling parameter for implementation. The obvious practical reasons are non-nominal flight times and ascent profiles. Stage separation is usually triggered if the launcher’s forward acceleration decreases below a specified threshold, e.g.,  $3 \text{ m/s}^2$ , which indicates the burnout of the solid rocket motor. However, uncertainties in the combustion process cause longer or shorter burn times. The results are later or earlier stage separations, respectively. Due to thrust perturbations, also the momentary launcher dynamics at current points in time  $t_i$  of the ascent would diverge continuously from the nominal dynamics at  $t_i$ , which were used to synthesize the controller  $\mathbf{K}(t_i)$ . Longer flight times can be accounted for by limiting the scheduling signal to the nominal separation time. However, the increasing mismatch between momentary launcher dynamics and momentary controller  $\mathbf{K}(t_i)$  persists. This mismatch is especially critical for flexible mode attenuation. The flexible modes’ natural frequencies depend on the launcher mass and therefore at a given time  $t_i$  on the past thrust profile. It is possible to replace time with an alternative scheduling parameter. Such a parameter must be strictly monotonically increasing so that a one-on-one map to time exists. A suitable choice for scheduling is the non-gravitational velocity, i.e. the integrated non-gravitational acceleration.

Non-gravitational velocity is the favorable scheduling parameter due to its direct dependence on the thrust and mass profile. For example, lower average thrust corresponds to lower velocities and higher fuel masses at times  $t_i$  than nominal. These lower velocities actually correspond to “earlier” nominal dynamics on the synthesis grid. Hence, a controller scheduled over non-gravitational velocity fits better to the actual launcher dynamics, which is beneficial for robustness of, e.g, the flexible mode attenuation. For implementation, the synthesis time grid and the corresponding controller dynamics are mapped onto the nominal ascent’s velocity profile. Non-gravitational velocity is then used as scheduling signal in the nonlinear simulation. For smoothness, the controller matrices in-between the explicitly calculated controller grid points are interpolated via PCHIPs. Note that thrust profiles which are on average higher than the one used for design can result in maximum velocities which exceed the final nominal velocity. Hence, the maximum value of the scheduling signal is limited to the final nominal velocity (corresponding to the controller  $\mathbf{K}(T)$ ).

## V. Results

### A. Nominal Performance Analysis

First, a simulation of the closed-loop model resulting from the interconnection of the nonlinear launcher dynamics and the LTV controller is conducted in Simulink. The closed loop is excited by the wind signal from the Vega mission VV05 as shown in Fig. 3. It induces a build-up of  $\bar{q}\alpha$  shown in Fig. 10, which stays at least a factor two below the  $\bar{q}\alpha$

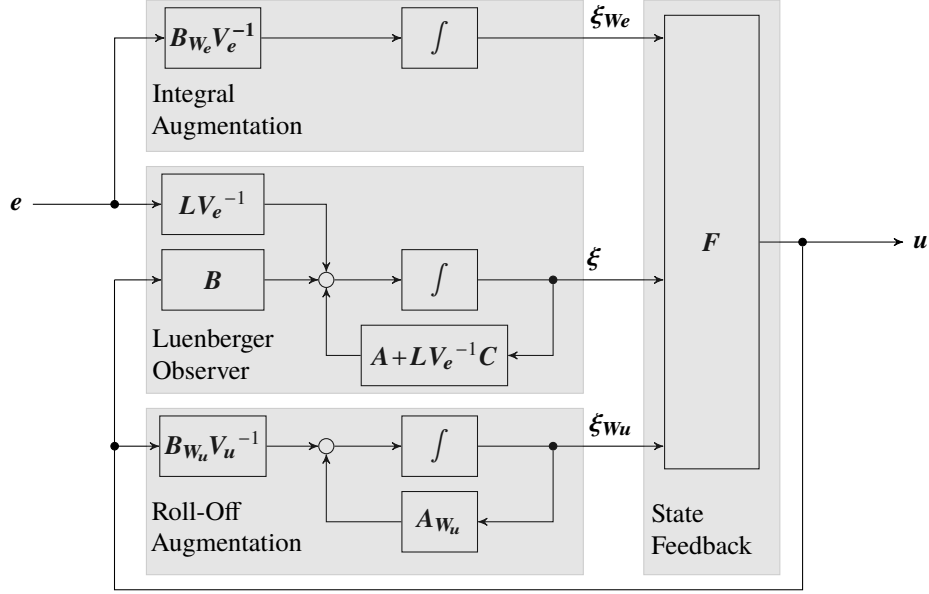


**Fig. 9 Observer-based controller with weights**

limit bound depicted in red. The control signal counteracts the disturbance and keeps the absolute pitch angle deviation  $\theta_{\text{err}}$  close to zero for the whole ascent and well below 0.5 deg at separation. The limit value at separation is indicated by the shortened red line in Fig. 10. During the whole ascent, the absolute drift rate  $\dot{z}$  does not exceed 20 m/s and the drift rate requirement at separation is fulfilled. The required TVC deflection remains below the saturation limit at all times. Thus, the controller displays excellent disturbance rejection and tracking. It is particularly noteworthy that no variation in performance is visible, although the unstable dynamics of the launcher vary significantly over time (see Fig. 6). The gravity turn maneuver takes 100.03 s, i.e., at this time forward acceleration falls below 3 s and separation is triggered. In conclusion, the proposed control design approach proves suitable for the time-varying launcher control problem with realistic disturbances. All performance requirements are achieved and the shorter flight time did not pose a problem.

## B. Robust Performance Analysis

The next simulation setup confirms the robustness of the LTV controller. It considers perturbed launcher parameters as well as realistic, wind disturbance. A significant amount of uncertainty arises from the launcher's aerodynamic parameters, mainly due to limited testing. Most aerodynamic data solely rely on numerical methods. Moreover, the launcher passes through the transonic regime ( $0.8 \leq Ma \leq 1.2$ ), for which calculating accurate aerodynamic parameters is complicated. One of the most challenging parameters to estimate is the center of aerodynamic pressure  $\delta_{l_{GP}}$  as the payload fairing causes a complex, turbulent airflow. Due to its significant contribution to the launcher's instability, a  $\pm 10\%$  uncertainty  $\delta_{l_{GP}}$  is included in  $l_{GP}$ . Additionally,  $\pm 10\%$  uncertainties in the aerodynamic force coefficients  $C_A$  and  $C_N$  are considered. The solid rocket motor's thrust is considered with a constant uncertainty  $\delta_T$  in the range of  $\pm 1.0\%$ . This uncertainty is attributed to the exhaust mass flow  $\dot{m}_{\text{ex}}$  in Eq. (11) and covers combustion errors. The thrust

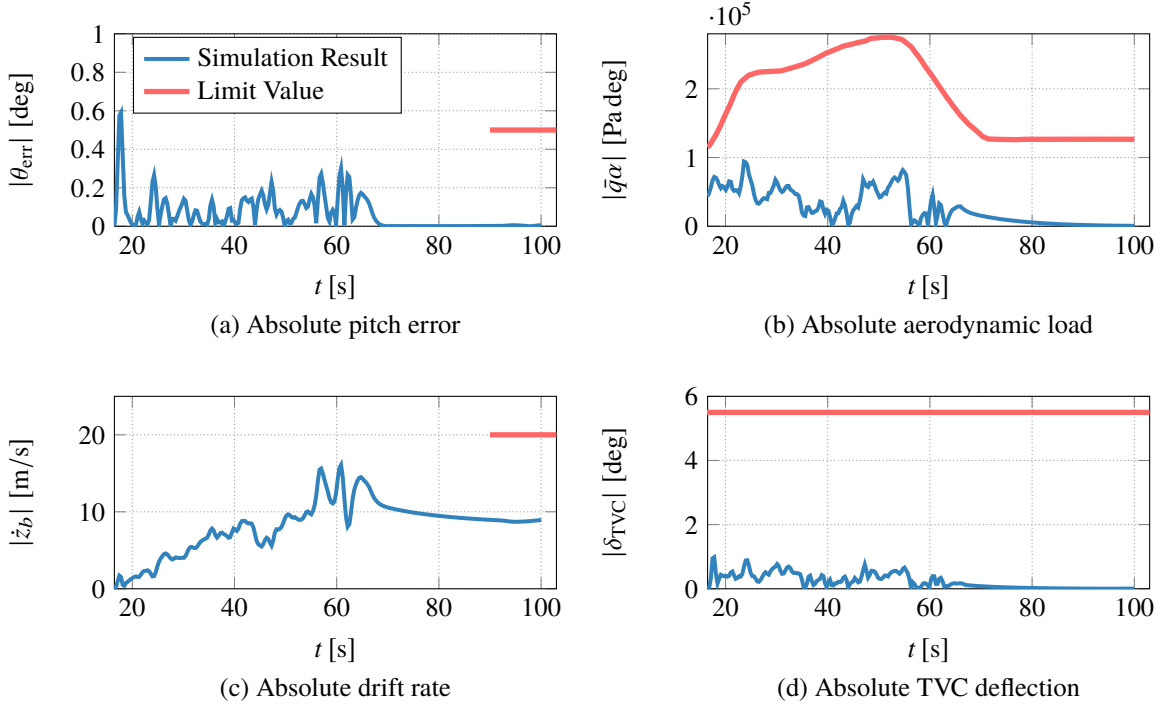


**Fig. 10** Nominal performance results under VV05 wind disturbance

perturbation directly affects the launcher’s velocity  $V$  and, thus, the dynamic pressure  $\bar{q}$  at a given point in time. It further indirectly affects the velocity through the variation in propellant consumption over time, the related change in weight and balance ( $G$ ,  $J_{yy}$ , and  $m$ ), and controllability ( $l_{CG}$ ). The thrust uncertainty is the main contributor to this uncertainty. Therefore, no explicit mass and balance uncertainties are modeled. As neither the velocity nor mass profile match the gravity turn trajectory calculated via Eq. (19), the launcher inevitably starts to drift away from its reference trajectory.

Regarding the launcher’s flexible motion, the eigenfrequencies of the flexible modes  $\omega_i$  are considered uncertain in a range of  $\delta_{\omega_i} \pm 5\%$ . They are further directly related to the launcher’s momentary mass and thus coupled with the thrust uncertainty. This coupling causes additional parameter perturbations.

Furthermore, the TVC dynamics are treated as uncertain. This uncertainty set covers up to 5% uncertainty in the TVC’s steady state gain  $\delta_{k_{TVC}}$ , damping ratio  $\delta_{\zeta_{TVC}}$ , and eigenfrequency  $\delta_{\omega_{TVC}}$ . A time delay of 30 ms is included between the pitch controller and the TVC accounting for computational delays. Tab. 3 summarizes all uncertainties considered in the controller analysis. The parameter variations in Tab. 3 are evaluated only on their respective vertices. Hence, a total of 1024 parameter combinations are analyzed.

The wind disturbance is generated by the proposed turbulence filter superimposed with a constant wind field as described in Section III.A.3. Thus, wind disturbances deviating from the VV05 profile but with similar spectral characteristics can be evaluated. Thirty-seven unique turbulence signals are considered resulting in 37888 simulation

runs.

**Table 3** Uncertainty set used for the controller analysis

Parameter	Notation	Range
$T$	$\delta_T$	$\pm 1\%$
$l_{GP}$	$\delta_{l_{GP}}$	$\pm 10\%$
$C_A$	$\delta_{C_A}$	$\pm 10\%$
$C_N$	$\delta_{C_N}$	$\pm 10\%$
$\omega_i$	$\delta_{\omega_i}$	$\pm 5\%$
$k_{TVC}$	$\delta_{TVC,k}$	$\pm 5\%$
$\zeta_{TVC}$	$\delta_{TVC,\zeta}$	$\pm 5\%$
$\omega_{TVC}$	$\delta_{TVC,\omega}$	$\pm 5\%$
Delay	$\tau$	30 ms

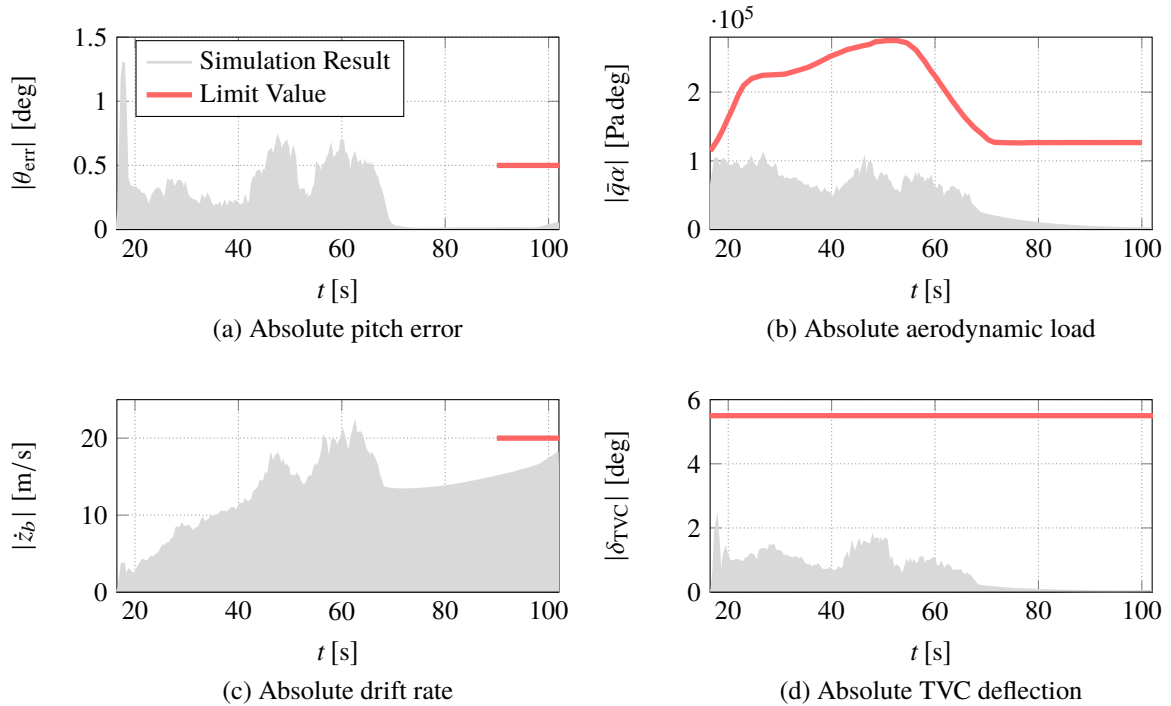


**Fig. 11** Monte Carlo simulation results

Fig. 11 shows the envelope of the simulation results (—) and the performance requirement (—). A shortened red line indicates that the requirement only needs to be fulfilled at separation. During the whole atmospheric ascent the tracking error  $\theta_{err}$  remains small with the maximum absolute deviation of 1.30 deg occurring at the start of the gravity turn caused by the fast initial wind build-up. Afterwards,  $|\theta_{err}|$  never exceeds 0.75 deg. The pitch deviation requirement at stage separation is fulfilled. Note that the stage-separation time varies between 97.64 s and 101.93 s. The absolute

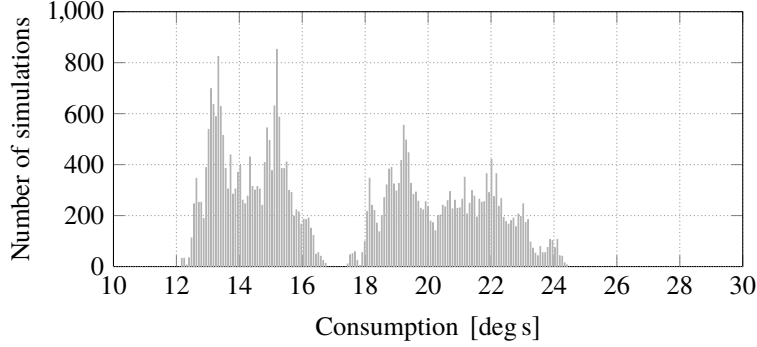


**Fig. 12 Histogram of consumption obtained from robust performance simulation**

drift rate  $|\dot{z}_b|$  does not exceed 20 m/s at engine cut-off as required. Overall, good drift performance is achieved as  $|\dot{z}_b|$  never exceeds 21.7 m/s. The maximum aerodynamic load occurs at 27 s with an absolute value of 108209 Pa deg, which is a factor of 2.1 below the local limit value indicated by (—). The lowest safety margin is 1.2 and occurs 17 s into the ascent. The safety factor never decreases below 2.6 in the most critical flight segment between 45 s and 65 s. Hence, the design exhibits excellent tracking and disturbance rejection in the high dynamic pressure region as intended by the applied time-varying weighting. The commanded control effort remains small over the whole trajectory, with a maximum absolute TVC deflection of 2.2 deg at around 18 s. It remains well below the saturation limit of 5.5 deg over the whole ascent. Fig. 12 shows a distribution of the calculated consumptions, i.e., the cumulative control effort along the trajectory. The maximum consumption is 25.3 deg s, which is almost ten times lower than the threshold of 250 deg s.

At all times, tight pitch angle control in combination with good load reduction is achieved regardless of the launcher dynamics and disturbances. This demonstrates the possibilities provided by a time-varying control design.

## VI. Conclusion

A finite horizon LTV design for a space launcher in atmospheric ascent is presented. The synthesis explicitly includes the launcher's time-varying dynamics as well as the variation of the control objectives along the ascent trajectory. A novel synthesis procedure for finite horizon LTV systems is applied, which yields a highly structured controller. The optimization problem is convex providing a norm optimal time-varying controller, based on a comprehensible weighting scheme solely based on principle system and control objective knowledge. The LTV approach therefore circumvents the solution of hard nonlinear optimization problems derived from the  $H_\infty$  framework. The concluding nonlinear analysis over a set of realistic wind disturbances and model perturbations demonstrates the suitability of LTV control for the ascent problem.

## Acknowledgments

This work has been partially funded by ESA under the Open Space Innovation Platform (OSIP) Co-Funded Research Program contract number 4000135/85/21/NL/GL/my. We would like to thank Dr. Samir Bennani, ESA technical officer, for his support.

## References

- [1] Clement, B., Duc, G., and Mauffrey, S., “Aerospace launch vehicle control: a gain scheduling approach,” *Control Engineering Practice*, Vol. 13, No. 3, 2005, pp. 333–347. <https://doi.org/10.1016/j.conengprac.2003.12.013>.
- [2] Silva, A. G., and Filho, W. C. L., “Launch Vehicle Attitude Control System using PD plus Phase Lag,” *IFAC Proc. Vol.*, Vol. 46, No. 19, 2013, pp. 48–53. <https://doi.org/10.3182/20130902-5-de-2040.00110>.
- [3] de la Llana, D. S., Bennani, S., Cruciani, I., and Aranda, J., “H-Infinity control of the VEGA Launch Vehicle first stage in presence of roll,” *IFAC Proc. Vol.*, Vol. 46, No. 19, 2013, pp. 54–59. <https://doi.org/10.3182/20130902-5-de-2040.00039>.
- [4] Ganet-Schoeller, M., and Desmariaux, J., “Structured  $H_\infty$  synthesis for flexible launcher control,” *IFAC-PapersOnLine*, Vol. 49, No. 17, 2016, pp. 450–455. <https://doi.org/10.1016/j.ifacol.2016.09.077>.
- [5] Navarro-Tapia, D., Marcos, A., and Bennani, S., “The VEGA launcher atmospheric control problem: A case for linear parameter-varying synthesis,” *J. of the Franklin Inst.*, 2021. <https://doi.org/10.1016/j.jfranklin.2021.07.057>.
- [6] Biertümpfel, F., Pifer, H., and Bennani, S., “Finite Horizon Worst Case Analysis of Launch Vehicles,” *IFAC-PapersOnLine*, Vol. 52, No. 12, 2019, pp. 31–36. <https://doi.org/10.1016/j.ifacol.2019.11.065>.
- [7] Biertümpfel, F., Bennani, S., and Pifer, H., “Time-Varying Robustness Analysis of Launch Vehicles Under Thrust Perturbations,” *Advanced Control For Applications*, 2021. <https://doi.org/10.1002/adc.2.93>.
- [8] Biertümpfel, F., Theis, J., and Pifer, H., “Observer-Based Synthesis of Finite Horizon Linear Time-Varying Controllers,” *2022 American Control Conference (ACC)*, IEEE, 2022. <https://doi.org/10.23919/acc53348.2022.9867184>.
- [9] Limebeer, D. J. N., Anderson, B. D. O., Khargonekar, P. P., and Green, M., “A Game Theoretic Approach to  $\mathcal{H}^\infty$  Control for Time-Varying Systems,” *SIAM J. Control Optim.*, Vol. 30, No. 2, 1992, pp. 262–283. <https://doi.org/10.1137/0330017>.
- [10] Theis, J., Pifer, H., and Seiler, P., “Robust Modal Damping Control for Active Flutter Suppression,” *J. Guidance, Control, Dynamics*, Vol. 43, No. 6, 2020, pp. 1056–1068. <https://doi.org/10.2514/1.g004846>.
- [11] Buch, J., and Seiler, P., “Finite horizon robust synthesis using integral quadratic constraints,” *Int. J. Robust Nonlinear Control*, Vol. 31, No. 8, 2021, pp. 3011–3035. <https://doi.org/10.1002/rnc.5431>.
- [12] Pifer, H., and Seiler, P., “Robustness analysis with parameter-varying integral quadratic constraints,” *2015 American Control Conference (ACC)*, IEEE, 2015. <https://doi.org/10.1109/acc.2015.7170725>.

- [13] J. Slotine, J., and Li, W., *Applied nonlinear control*, Prentice Hall, Englewood Cliffs, N.J, 1991.
- [14] Biertümpfel, F., and Pfifer, H., “Worst Case Gain Computation of Linear Time-Varying Systems over a Finite Horizon,” *2018 IEEE Conference on Control Technology and Applications*, 2018. <https://doi.org/10.1109/ccta.2018.8511591>.
- [15] Biertümpfel, F., Theis, J., and Pfifer, H., “Robust Observer-Based Space Launcher Control With Time-Varying Objectives,” *Proceedings of the 2022 CEAS EuroGNC Conference*, 2022.
- [16] Tadmor, G., “Input/output norms in general linear systems,” *Int. J. Control*, Vol. 51, No. 4, 1990, pp. 911–921. <https://doi.org/10.1080/00207179008934104>.
- [17] Skogestad, I., Sigurd; Postlethwaite, *Multivariable Feedback Control*, 2<sup>nd</sup> ed., John Wiley and Sons, 2005.
- [18] Khargonekar, P. P., Nagpal, K. M., and Poolla, K. R., “ $H_\infty$  Control with Transients,” *SIAM J. Control Optim.*, Vol. 29, No. 6, 1991, pp. 1373–1393. <https://doi.org/10.1137/0329070>.
- [19] O’Brien, R., and Iglesias, P., “Robust Controller Design for Linear, Time-Varying Systems,” *Eur. J. Control*, Vol. 5, No. 2-4, 1999, pp. 222–241. [https://doi.org/10.1016/s0947-3580\(99\)70157-3](https://doi.org/10.1016/s0947-3580(99)70157-3).
- [20] Miele, A., *Flight Mechanics Theory of Flight Paths*, Addison-Wesley Publishing Company Inc., 1962.
- [21] Greensite, A. L., “Analysis and Design of Space Vehicle Flight Control Systems. Volume VII - Attitude Control During Launch,” Tech. rep., NASA Marshall Space Flight Center; Huntsville, AL, 1967.
- [22] Greensite, A. L., “Analysis and Design of Space Vehicle Flight Control Systems. Volume I - Short Period Dynamics,” Tech. rep., NASA Marshall Space Flight Center; Huntsville, AL, 1967.
- [23] “Manual of the ICAO Standard Atmosphere,” Tech. rep., May 1954.
- [24] NIMA, “Department of Defense World Geodetic System 1984, Its Definition and Relationships With Local Geodetic Systems,” Tech. Rep. 3, Jul. 1997.
- [25] Simplicio, P., Bennani, S., Marcos, A., Roux, C., and Lefort, X., “Structured Singular-Value Analysis of the Vega Launcher in Atmospheric Flight,” *J. Guidance, Control, Dynamics*, Vol. 39, No. 6, 2016, pp. 1342–1355. <https://doi.org/10.2514/1.g000335>.
- [26] Hoblit, F. M., *Gust Loads on Aircraft: Concepts and Applications*, American Institute of Aeronautics and Astronautics, 1988. <https://doi.org/10.2514/4.861888>.
- [27] Wiesel, W. E., *Spaceflight dynamics*, 3<sup>rd</sup> ed., Beavercreek, Ohio : Aphelion Press, 2010.
- [28] Wie, B., *Space Vehicle Dynamics and Control, Second Edition*, American Institute of Aeronautics and Astronautics, 2008. <https://doi.org/10.2514/4.860119>.
- [29] Theis, J., and Pfifer, H., “Observer-based synthesis of linear parameter-varying mixed sensitivity controllers,” *Int. J. Robust Nonlinear Control*, Vol. 30, No. 13, 2020, pp. 5021–5039. <https://doi.org/10.1002/rnc.5038>.

- [30] Green, M., and Limebeer, D. J. N., *Linear Robust Control*, Prentice-Hall, Inc., Upper Saddle River, NJ, USA, 1995.
- [31] MATLAB, *R2020b*, The MathWorks Inc., Natick, Massachusetts, 2020.
- [32] Abou-Kandil, H., Freiling, G., Ionescu, V., and Jank, G., *Matrix Riccati Equations in Control and Systems Theory*, Birkhäuser Basel, 2003. <https://doi.org/10.1007/978-3-0348-8081-7>.
- [33] Theis, J., Sedlmair, N., Thielecke, F., and Pfifer, H., “Observer-based LPV Control with Anti-Windup Compensation: A Flight Control Example,” *IFAC-PapersOnLine*, Vol. 53, No. 2, 2020, pp. 7325–7330. <https://doi.org/10.1016/j.ifacol.2020.12.988>.